JOURNAL OF GEOPHYSICAL RESEARCH, VOL. 114, D10304, doi:10.1029/2008JD011462, 2009

Wintertime water vapor in the polar upper mesosphere and lower thermosphere: First satellite observations by Odin submillimeter radiometer

S. Lossow,[1,2] J. Urban,[2] H. Schmidt,[3] D. R. Marsh,[4] J. Gumbel,[1] P. Eriksson,[2] and D. Murtagh[2]

Received 12 November 2008; revised 13 March 2009; accepted 24 March 2009; published 22 May 2009.

[1] In this paper we present Odin submillimeter radiometer (Odin/SMR) water vapor measurements in the upper mesosphere and lower thermosphere with focus on the polar latitudes in winter. Measurements since 2003 have been compiled to provide a first overview of the water vapor distribution in this altitude range. Our observations show a distinct seasonal increase of the water vapor concentration during winter at a given altitude above 90 km. Above 95 km the observations exhibit the annual water vapor maximum during wintertime. Model simulations from the Hamburg Model of the Neutral and Ionized Atmosphere (HAMMONIA) and the Whole Atmosphere Community Climate Model version 3 (WACCM3) show results that are very similar to the observations. We suggest that the observed increase in water vapor during winter is mainly caused by a combination of upwelling of moister air from lower altitudes and diffusion processes. Distinct interhemispheric differences in the winter water vapor distribution in the upper mesosphere and lower thermosphere can be observed, both in the observations and the model results. The seasonal water vapor increase in the polar regions is much more pronounced in the Southern Hemisphere winter where higher concentrations can be observed. This observation is most likely due to interhemispheric differences in the underlying dynamics and diffusion processes.

Citation: Lossow, S., J. Urban, H. Schmidt, D. R. Marsh, J. Gumbel, P. Eriksson, and D. Murtagh (2009), Wintertime water vapor in the polar upper mesosphere and lower thermosphere: First satellite observations by Odin submillimeter radiometer, *J. Geophys. Res.*, *114*, D10304, doi:10.1029/2008JD011462.

1. Introduction

[2] Water vapor is the most important greenhouse gas and plays a fundamental role in the climate system and for the chemistry of the Earth's atmosphere. In the middle atmosphere water vapor is also a particularly suitable tracer for dynamical processes, since the lifetimes of chemical and transport processes are comparable. In the last ~30 years a series of satellite-borne and ground-based measurements have established a general picture of the water vapor distribution in the middle atmosphere [e.g., *Taylor et al.*, 1981; *Fischer et al.*, 1981; *Remsberg et al.*, 1984; *Reber et al.*, 1993; *Mote et al.*, 1996; *Nedoluha et al.*, 1996; *Summers et al.*, 1997; *Chandra et al.*, 1997; *Randel et al.*, 1998; *Seele and Hartogh*, 1999; *Summers et al.*, 2001; *Hervig et al.*, 2003; *Thomason et al.*, 2004; *Nassar et al.*, 2005; *Urban et al.*, 2007].

[3] Water vapor enters the middle atmosphere primarily by vertical transport through the tropical tropopause layer (TTL) [e.g., *Holton et al.*, 1995; *Fueglistaler et al.*, 2009]. The low temperatures inside this layer cause a strong reduction of the water vapor concentration by freeze-drying and subsequent sedimentation of ice particles. In the stratosphere the water vapor concentration increases with altitude. This increase is due to the production of water vapor by the oxidation of methane. This production outweighs the main sink process of water vapor in the stratosphere, i.e., the reaction with $O(^1D)$. With increasing altitude the destruction of water vapor by photodissociation becomes increasingly important. Above about 70 km the photodissociation is primarily caused by solar Lyman-α radiation [*Brasseur and Solomon*, 1998]. The balance between these production and loss processes can be found roughly in the upper stratosphere/lower mesosphere region, consequently resulting in a water vapor maximum at those altitudes. In the mesosphere, the water vapor concentration decreases generally with altitude, since additional production processes are usually missing [*Brasseur and Solomon*, 1998].

[4] Two pronounced deviations from the described general water vapor distribution in the mesosphere can be

[1]Department of Meteorology, Stockholm University, Stockholm, Sweden.
[2]Department of Radio and Space Science, Chalmers University of Technology, Göteborg, Sweden.
[3]Atmosphere in the Earth System, Max Planck Institute for Meteorology, Hamburg, Germany.
[4]Atmospheric Chemistry Division, National Center for Atmospheric Research, Boulder, Colorado, USA.

0148-0227/09/2008JD011462$09.00

observed at certain times and locations. In addition to the maximum around the stratopause a second water vapor maximum can be found both in the tropics around equinox and in the polar regions during summer in the altitude range between 65 km and 75 km [*Nedoluha et al.*, 1996; *Summers et al.*, 1997; *Seele and Hartogh*, 1999]. This maximum arises from an interplay of upwelling winds and autocatalytical water vapor formation from the molecular hydrogen reservoir during the period of strongest insolation [*Sonnemann et al.*, 2005]. Another maximum can be observed at polar latitudes during the summer season in a small layer around 82 km. This peak is caused by the redistribution of water vapor by sedimenting ice particles forming polar summer mesosphere echoes (PMSE) and noctilucent clouds (NLC) [*Summers et al.*, 2001; *von Zahn and Berger*, 2003]. These ice particles can form by heterogeneous nucleation near the very cold mesopause (~88 km), typically at temperatures below 150 K. Around 82 km the sedimenting ice particles encounter warmer temperatures, which cause a rapid sublimation and the release of the consumed water in a small layer.

[5] So far, satellite-borne and ground-based water vapor measurements were usually limited to a top altitude in the 80-km to 90-km region. Only on very rare occasions, rocket-borne measurements have explored the water vapor content at altitudes even above 90 km [*Arnold and Krankowsky*, 1977; *Grossmann et al.*, 1985; *Kopp*, 1990], so that the current picture of the water vapor distribution above 90 km is entirely determined by model simulations. In this paper we present for the first time global water vapor measurements up to an altitude of 110 km as observed by the submillimeter radiometer (SMR) aboard the Odin satellite. This instrument passively scans the thermal emissions of several trace gases at the atmospheric limb. Profiles covering these high altitudes are retrieved from the 557 GHz emission line of water vapor. Here we put our focus on the winter season at polar latitudes. Our observations show a distinct seasonal increase of the water vapor concentration during winter at altitudes above 90 km. Above about 95 km the annual water vapor maximum can be found during the winter season. This behavior is different than the subjacent part of the mesosphere, where the annual water vapor maximum can be observed during summertime, caused by a gravity wave driven meridional circulation, with upwelling over the summer pole and downwelling over the winter pole.

[6] The further organization of this paper is as follows. In section 2 we give a brief overview of the Odin/SMR water vapor measurements, retrieval and data quality. The observations are presented in section 3, while we focus on model results in section 4. The results are subsequently discussed and summarized in section 5.

2. Odin/SMR Water Vapor Measurements

[7] The Odin satellite has been launched on 20 February 2001 into a polar, sun synchronous and near-terminator orbit at an altitude of around 600 km, orbiting the Earth about 15 times a day. Odin carries two instruments aboard, one of them is the submillimeter radiometer. The SMR instrument measures thermal emissions at the atmospheric limb in several frequency bands between 486 GHz and 581 GHz and around 119 GHz [*Frisk et al.*, 2003].

2.1. Measurements of the 557-GHz Band and Its Retrieval

[8] The water vapor data in the upper mesosphere and lower thermosphere are based on measurements of the 557-GHz water vapor emission line (the line center is located at 556.936 GHz). General information about the Odin/SMR measurements of the 557-GHz band and its retrieval are described by *Urban et al.* [2007] and *Lossow et al.* [2007]. Here we will only focus on details relevant for the upper mesosphere/lower thermosphere data set. The measurements in this altitude range are part of stratosphere-mesosphere scans. In 2001 and 2002 these scans were scheduled to cover the altitude range between 7 km and 100 km. Since 2003 the measurements are performed up to a top tangent height of 110 km, while especially in 2005 and 2006 the measurements frequently exceeded this top height. The limiting factor of the water vapor retrieval at altitudes above 90 km is given by the signal-to-noise ratio (SNR) of the measurement and the volume mixing ratio of water itself. The statistical error of individual retrieved profiles can be on the order of 40% to 50% at 90 km and even exceed 100% above 100 km. Typically a SNR of 25 corresponds to a statistical error of about 50% for a single profile retrieved, while a SNR of about 5 corresponds to a statistical error of about 100% in the Odin/SMR retrieval. However there is no simple linear connection between the SNR and the retrieved statistical error. It is much more a complex tradeoff between the vertical resolution, weighting factors and error estimates of the retrieval. Above 105 km the SNR is typically on the order of 1. Hence, in order to get sensible results in the upper mesosphere and especially in the lower thermosphere averaging over many retrieved profiles is necessary. The vertical resolution of the retrieval is maintained at about 3 km up to the altitude of 110 km.

2.2. Data Quality

[9] For this study we use the official Odin/SMR level-2 data, derived with the retrieval version 2.1 [*Lossow et al.*, 2007]. The quality of the retrieved water vapor data has been assessed by a comparison to correlative measurements of the Fourier Transform Spectrometer (FTS) instrument aboard the Canadian ACE (Atmospheric Chemistry Experiment) satellite [*Bernath et al.*, 2005]. This instrument performs solar occultation measurements of the atmospheric extinction in the midinfrared. The comparison with the ACE/FTS retrieval version 2.2 [*Boone et al.*, 2005] reveals on the global scale a dry bias of the Odin/SMR data in the entire mesosphere up to an altitude of 89 km. This is the uppermost altitude were water vapor concentrations are retrieved from the ACE/FTS measurements [*Carleer et al.*, 2008]. The bias is typically (0.4 ± 0.2) ppmv. Above 89 km we cannot give any statement about the Odin/SMR water vapor data quality so far, owing to the lack of correlative measurements. We will return to this topic in section 4 when we compare our measurements with model results.

[10] An important issue in the upper mesosphere and lower thermosphere may be systematic errors arising from

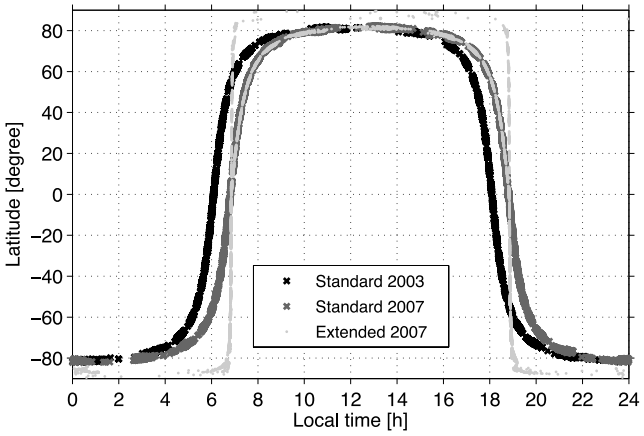

Figure 1. The local time coverage of the Odin measurements as function of latitude. Black crosses are used for the coverage in 2003, dark grey crosses for the coverage in 2007. Light grey dots show an example of the local time coverage in 2007 when the Odin measurements were performed off the orbital track and extended toward the pole. These off-track measurements were regularly performed since 2004 during the Southern Hemisphere summer season. In the Southern Hemisphere the measurements are always extended toward the pole during this time, and in the northern Hemisphere only when permitted by Sun angle constraints.

uncertainties in the radiometric calibration, since the observed water vapor concentrations at these altitudes are very low. In order to understand the size of those errors we conducted a sensitivity study for the polar regions and the maximum uncertainty of the Odin/SMR calibration scheme as estimated by *Urban et al.* [2005]. These estimates are a rather conservative choice, since more recent investigations indicate smaller uncertainties in the radiometric calibration [*Ekström et al.*, 2007]. This sensitivity study revealed a maximum error of about 0.03 ppmv at altitudes above 90 km due to uncertainties in the radiometer calibration. In addition systematic errors, which may arise from an accounted but not completely understood issue in the Odin/SMR autocorrelator calibration, need to be kept in mind. This calibration issue concerns in general altitudes above 50 km and is expressed by too low intensities in the frequency channels at and close to the center of the water vapor emission line, which correspond in turn to lower retrieved water vapor concentrations. Up to an altitude of about 90 km the Odin/SMR measurements of the 557-GHz band allow besides the water vapor retrieval also the derivation of temperature information [*Lossow et al.*, 2007]. Above climatological temperature information has to be used for the water vapor retrieval, which may also give rise to systematic errors. The Odin/SMR retrieval uses the CIRA (COSPAR International Reference Atmosphere) data set from 1986 at these altitudes [*Fleming et al.*, 1990]. We have investigated the influence of the climatological temperature on the water vapor retrieval by increasing and decreasing the temperature by 10 K, respectively. In average the influence is less than 0.01 ppmv in the altitude range between 90 km and 110 km during all seasons. Overall, we estimate that the systematic error of the derived water vapor is on the order of 10% to 20%. In the discussion of our results we will restrict ourselves to water vapor concentrations down to 0.1 ppmv, which appears to be a safe lower limit given the systematic errors of the retrieval discussed above.

2.3. Data Set and Handling

[11] For the current study we employed all data which are available since 2003, when the measurements reached up to 110 km and higher. We use only data taken with the measurement configuration "frequency mode 19." This configuration is one of in total three configurations used to measure the 557-GHz band, which differ in the frequency band covered and the radiometer frontend used. The "frequency mode 19" configuration has been used most often and throughout the Odin/SMR aeronomy mission and is the most optimized for the measurements of the 557-GHz band. We implement only profiles which have been flagged as usable for scientific analysis by the retrieval quality control. This quality control is based on different parameters, such as the convergence and the cost function of the retrieval (chi-square statistical analysis), the Levenberg-Marquardt parameter (regularization of the nonlinear retrieval) and the retrieved pointing offset. In addition we require a measurement response of at least 70% of the retrieved values, in order to minimize the influence of the a priori information needed for the OEM (Optimal Estimation Method) retrieval [*Rodgers*, 2000].

[12] Furthermore we implemented only data taken poleward up to a latitude of 82.5 degrees, which is the maximum latitude covered by the Odin measurements along the orbital track. Since 2004, Odin performs measurements pointing off the orbital track during the Southern Hemisphere summer season, which extend the latitude coverage toward the pole. In the Southern Hemisphere the measurements are always extended toward the pole during this time, in the Northern Hemisphere only when permitted by Sun angle constraints. To avoid any possible interhemispheric differences as an artefact due to this different latitude coverage we have constrained the data set to its usual latitude limit of 82.5 degrees.

[13] Another important aspect to keep in mind for the interpretation of the results is the local time (LT) coverage of the Odin measurements, which is shown in Figure 1. Owing to its Sun-synchronous orbit, Odin performs measurements in general only at two local times at a given latitude, i.e., one local time on the ascending node and a second one on the descending node. At the highest latitudes the satellite passes quickly through several local times. Owing to the decreasing altitude of the Odin orbit over the years, caused by atmospheric drag, the local time coverage has changed slightly. The black crosses show the local time coverage for 2003, while the dark grey crosses show the coverage for 2007. In the beginning of the Odin mission the equator was passed at 1800 LT on the ascending node and 0600 LT on the descending node. In 2007 the equator was passed about 45 min later. The light grey dots show an example of the local time coverage from 2007 when the Odin measurements were performed off track and extended toward the poles. In the upper mesosphere and lower thermosphere, water vapor will show a diurnal variation, which is essentially determined by atmospheric

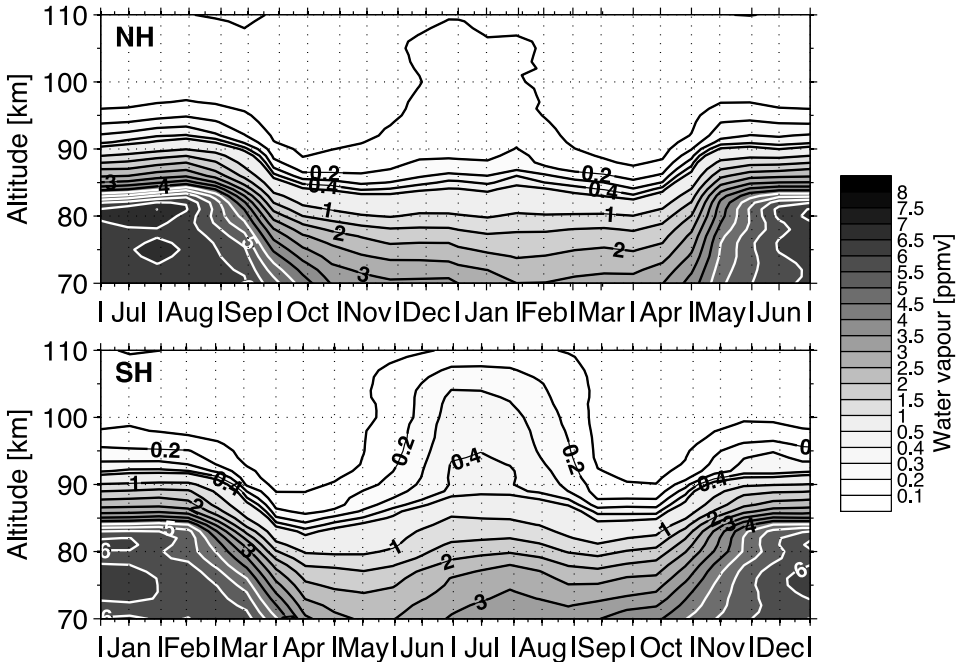

Figure 2. The annual mean water vapor distribution in the polar region between 60° and 82.5° in the (top) Northern Hemisphere and (bottom) Southern Hemisphere as observed by Odin/SMR. All available data since 2003 have been included. The data have been interpolated on a 15-day time grid, where the single data points describe a mean over 30 days. Note that we adapted the time grid so that the wintertime is in the center of each panel.

tidal waves. These global-scale waves are thermally driven by the periodic absorption of solar radiation throughout the atmosphere, primarily the absorption of infrared radiation by water and water vapor in the troposphere and ultraviolet radiation by stratospheric ozone. Also large-scale latent heat release by convective systems and nonlinear interactions between global-scale waves are important excitation sources of atmospheric tidal waves [e.g., *Chapman and Lindzen*, 1970; *Hagan and Forbes*, 2002, 2003]. Given the local time coverage of the Odin satellite, tidal signatures are embedded in the measured data, which need to be considered in the interpretation of the results. Measurements of tidal variations in water vapor are very rare in general and so far not available for the altitude range of interest here. A possible solution is to account for the tidal signatures with model data, which indicate relatively small amplitudes in the polar region [e.g., *Hagan et al.*, 1999]. However, unlike in the tropics and midlatitudes the knowledge about tides is rather limited in the polar areas [e.g., *Wu et al.*, 2006]. First global tide measurements have been reported rather recently [*Killeen et al.*, 2006]. With this background we hesitate to apply any tidal correction in this first presentation of water vapor measurements in the polar upper mesosphere and lower thermosphere and such correction will be part of a future study.

[14] The available profiles have first of all been interpolated onto a 1-km altitude grid. To describe the annual water vapor distribution in the polar region we implemented data in the latitude range 60° to 82.5° and averaged the data set onto a 15-day time grid. Every grid point describes a mean over 30 days, so that the single data points are not completely independent of each other in time. The statistical error of these average profiles is on the order of 15% at 100 km and up to 30% to 50% at 110 km. The highest uncertainties coincide with the lowest water vapor concentrations. For the description of the latitudinal distribution, we implemented data from December to February and June to August respectively and averaged the data set over a latitude range of 10 degrees on a 5 degree latitude grid. Hence, the single data points are not completely independent of each other in the latitude domain. The statistical error of latitudinal average profiles is on the order of 10% at 100 km and between 20% and 60% at 110 km.

3. Observations

[15] Figure 2 shows the mean annual water vapor distribution in the polar region (60° to 82.5° latitude) in the Northern Hemisphere (Figure 2, top) and Southern Hemisphere (Figure 2, bottom) using all available data since 2003. Below 90 km the annual cycle is characterized by a summertime maximum. This maximum arises owing to the gravity wave driven meridional pole-to-pole circulation, comprising upwelling over the summer pole and downwelling over the winter pole. Above 90 km the water vapor concentration exhibits a distinct seasonal increase during winter. Above 95 km the concentrations observed during summertime are actually lower than those during winter; that is, the annual maximum can be found in wintertime in this altitude range. It should also be noted that in the altitude range between 90 km and 100 km a clear semiannual variation is visible. The absolute annual minimum water

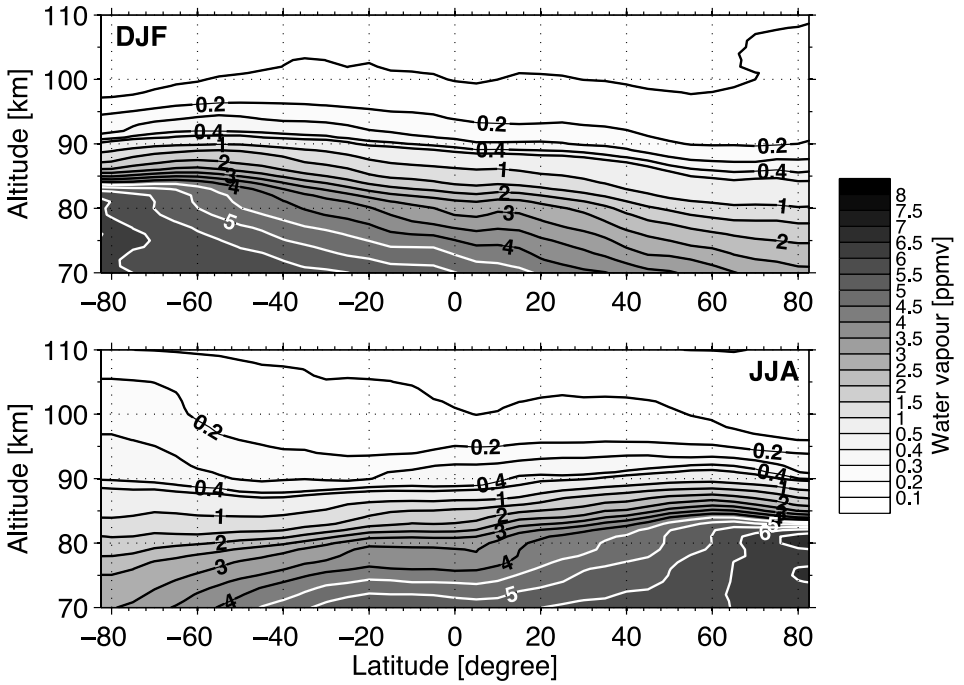

Figure 3. The mean latitudinal distribution of water vapor during the time period (top) December to February (DJF) and (bottom) June to August (JJA) as derived from Odin/SMR measurements. The data have been interpolated on a 5 degree latitude grid, where the single data points describe a mean over a latitude range of 10 degrees.

vapor concentrations can be observed around the equinoxes in this altitude region.

[16] Distinct differences can be observed between the Northern and Southern Hemisphere. The water vapor increase in winter is much more pronounced in the Southern Hemisphere where clearly higher concentrations can be observed. At 100 km a water vapor concentration of slightly above 0.35 ppmv can be observed in the Southern Hemisphere, while the concentration is just above 0.1 ppmv in the Northern Hemisphere. Figure 2 might imply that the seasonal increase of water vapor during winter lasts over a longer period of time in the Southern Hemisphere. However, this appears not to be true if we also incorporate the water vapor concentrations below 0.1 ppmv, which are not resolved in Figure 2. In the Southern Hemisphere the water vapor increase ranges typically from April to September/October, and in the Northern Hemisphere from October to March, with peak values shortly after winter solstice.

[17] Figure 3 provides an overview of the latitudinal water vapor distribution for the time periods December to February (DJF, Figure 3, top) and June to August (JJA, Figure 3, bottom). The seasonal increase of water vapor during wintertime is visible in a broader latitude band in the Southern Hemisphere as compared to its northern counterpart, connected to the higher water vapor concentrations observed in this hemisphere.

[18] Since local time variations due to atmospheric tidal waves are embedded in the data set, we performed in addition a comparison of the annual water vapor distributions using data from different local time periods. In the Northern Hemisphere we compared the local time period between 0600 LT and 0900 LT (descending node) with the local time period between 1600 LT and 1900 LT (ascending node). These two local time periods have been chosen since they comprise measurements in the same latitude range on the ascending and descending node, respectively (see Figure 1). This eliminates any local time differences based on a different latitude coverage. In the Southern Hemisphere we used the local time periods 0400 LT to 0700 LT and 1800 LT to 2100 LT, respectively. In the altitude range of interest, above 90 km, we do not observe significant differences in the annual distribution between the two local time periods used in the Northern Hemisphere. In the Southern Hemisphere during winter we observe slightly more water vapor (less than 0.1 ppmv) in the morning in the altitude range between 90 km and 105 km.

[19] We note that clear water vapor differences can be observed below 90 km in both hemispheres between the two local time periods considered. In the Northern Hemisphere we observe in general less water vapor in the local time period from 0600 LT to 0900 LT as compared to the period from 1600 LT to 1900 LT. In the Southern Hemisphere on the other hand we usually observe more water vapor in the local time period from 0400 LT to 0700 LT as compared to the period from 1800 LT to 2100 LT. The differences can be as high as a half ppmv. There is only one significant deviation from the behavior described above. In both hemispheres the situation reverses during summertime in the altitude range between 85 km and 90 km, where NLC and PMSE are formed. Here we observed more water vapor between 0600 LT and 0900 LT in the Northern Hemisphere and between 1800 LT and 2100 LT in the Southern

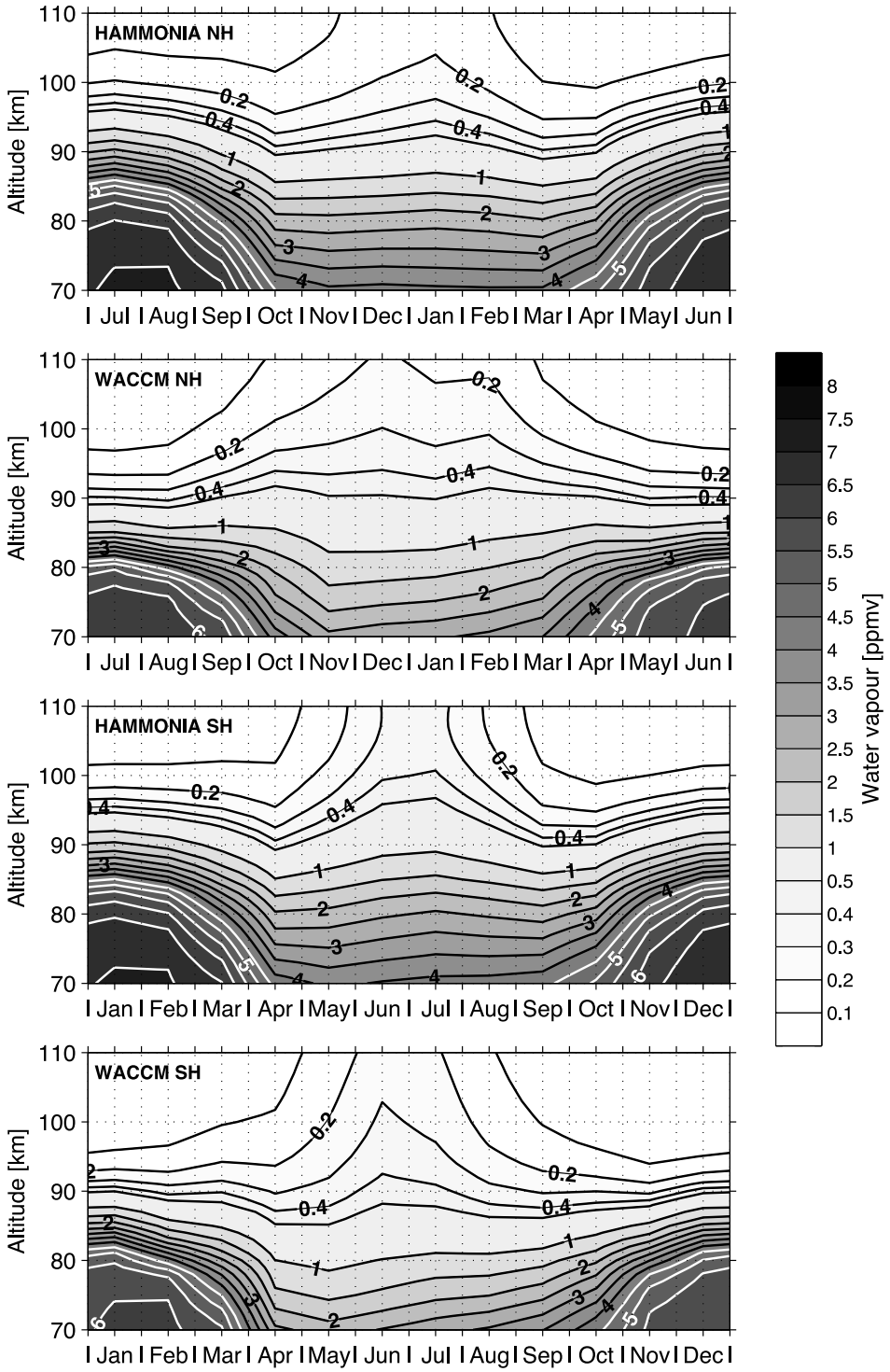

Figure 4. Like Figure 2 but here for HAMMONIA and WACCM3 results. Note again that we adapted the time grid in a way so that the wintertime is in the center of each panel.

Hemisphere. These differences can amount up to 0.7 ppmv and might be addressed in detail elsewhere.

4. Model Results

[20] Since our measurements are the first of their kind it is a natural step to compare them to model results, not only for validation but also to put the measurements into a larger perspective. Future model versions may also benefit from our measurements. Here we use the Hamburg Model of the Neutral and Ionized Atmosphere (HAMMONIA) and the Whole Atmosphere Community Climate Model version 3 (WACCM3). Both models are general circulation models (GCMs) with coupled chemistry. HAMMONIA ranges from

the surface up to a pressure level of 1.7×10^{-7} hPa ($\sim$250 km) employing 67 vertical levels. WACCM3 comprises 66 vertical levels up to a pressure of 4.5×10^{-6} hPa ($\sim$145 km). For detailed information about HAMMONIA the reader is referred to *Schmidt et al.* [2006], and for WACCM3 to *Garcia et al.* [2007]. The results from both models are given as monthly means. They describe diurnally averaged conditions and represent average conditions over a solar cycle. The HAMMONIA results presented here are from a time-slice experiment using greenhouse gas conditions of the 1990s. Two simulations have been averaged together. One simulation represented solar maximum conditions, while the second one was representative for solar minimum conditions. The WACCM3 data used here have been adapted to the available HAMMONIA data. The WACCM3 data are based on an average of simulations over the time period from 1990 to 2000, covering a complete solar cycle.

[21] The solar cycle has an importance for the absolute water vapor concentrations among many other things [e.g., *Chandra et al.*, 1997; *Sonnemann and Grygalashvyly*, 2005; *Schmidt et al.*, 2006]. The flux of Lyman-α radiation, which dominates the water vapor loss above 70 km (see section 1), increases typically by over 60% from the solar minimum to the solar maximum. Hence higher water vapor concentrations can be observed during the solar minimum than under solar maximum conditions. According to the HAMMONIA simulations the relative increase in the water concentration from solar maximum to solar minimum conditions amounts to about 30% right above 80 km and to approximately 60% at about 110 km in polar region during winter [see *Schmidt et al.*, 2006, Figure 12]. The solar cycle had a maximum in 2001/2002 and has been on a minimum in 2008. The average of the implemented Odin/SMR data set (2003–2008) will therefore not exactly describe average solar cycle conditions, but will be weighted somewhat toward solar minimum conditions. Hence there is a likelihood that the Odin/SMR results should exhibit somewhat higher water vapor concentration as the model results, which represent solar cycle average conditions. This needs to be kept in mind for the comparison of the absolute water vapor concentrations between the Odin/SMR measurements and the model results, later in this section.

[22] Similar to Figure 2, Figure 4 shows the mean annual water vapor distribution in the polar latitude range between 60° and 82.5° in the Northern and Southern Hemisphere as simulated by HAMMONIA and WACCM3. Both models clearly show the seasonal water vapor increase during wintertime at altitudes above 90 km to 95 km. In the WACCM3 simulations this increase ranges over a longer period of time as compared to the Odin measurements (see Figure 2). In the Northern Hemisphere the water vapor increase occurs from August to April/May and in the Southern Hemisphere typically from March/April to October/November. As the Odin observations the HAMMONIA simulations exhibit the seasonal increase from October and March in the Northern Hemisphere and from April to September/October in the Southern Hemisphere. HAMMONIA shows higher wintertime peak water vapor concentrations in the Southern Hemisphere, both at 100 km and 110 km, with respect to its Northern Hemisphere equivalent. This is also valid for the WACCM3 results, however the differences in the peak concentrations between both hemispheres are rather small. In the altitude range between 90 km and 100 km the HAMMONIA simulations show consistent with the Odin/SMR observations a clear semiannual variation in the water vapor distribution. The maxima can be observed shortly after the solstices, and the minima closely to the equinoxes. In the WACCM3 results this behavior is however not apparent.

[23] Figure 5 gives an overview of the latitudinal distribution of water vapor during the Northern (DJF) and Southern Hemisphere winter (JJA) as described by both models, HAMMONIA and WACCM3. Figure 5 shows that the water vapor increase during winter is visible to a greater part in the polar regions, but also at midlatitudes. In the summer hemisphere and the tropics, HAMMONIA usually exhibits more water vapor than WACCM3 at altitudes above 90 km. At the equator the contour lines tend to rise in the HAMMONIA results, while they show a distinct dip in the WACCM3 results. As in the Odin/SMR observations, interhemispheric differences can be observed in the model simulations. HAMMONIA shows higher water vapor concentrations above 90 km during the winter season in the Southern Hemisphere polar region as compared to the Northern Hemisphere. In the WACCM3 results the water vapor concentrations are rather similar in the polar areas of both hemispheres, actually with slightly higher values in the Northern Hemisphere averaged over the winter season. The seasonal increase is also visible in a broader latitude range during the Northern Hemisphere winter season in the WACCM3 simulations. This is opposite to the HAMMONIA results, where the increase is visible in a broader latitude range in the Southern Hemisphere during wintertime.

[24] Figure 6 shows a comparison of the Odin measurements in the upper mesosphere and lower thermosphere with HAMMONIA and WACCM3 results. Figure 6 (left) shows the mean water vapor profiles for January in the Northern Hemisphere and Figure 6 (right) shows the mean profiles for July in the Southern Hemisphere. As before, these mean profiles comprise data in the latitude range 60° to 82.5°. In the Northern Hemisphere in January the Odin/SMR observations exhibit lower water vapor concentrations in the entire altitude range considered here as compared to HAMMONIA and WACCM3. Above 90 km it is usually a factor 2–3 less water vapor. HAMMONIA shows more water vapor than WACCM3 below 95 km, higher up both models show very similar concentrations. In the Southern Hemisphere in July the water vapor concentrations observed by Odin lie between the model results almost in the entire altitude range addressed here, with HAMMONIA on the high and WACCM3 on the low side. Just at the uppermost altitudes the Odin/SMR observations show lower water vapor concentrations compared to WACCM3. Above 90 km the HAMMONIA water vapor concentrations are typically a factor of 2 higher than the WACCM3 concentrations. At 110 km the Odin/SMR exhibit a factor 2–3 lower water vapor concentrations as the model results, similar to the observed behavior in January in the Northern Hemisphere.

5. Discussion and Summary

[25] Odin/SMR observations provide for the first time an overview of the annual water vapor distribution in the upper

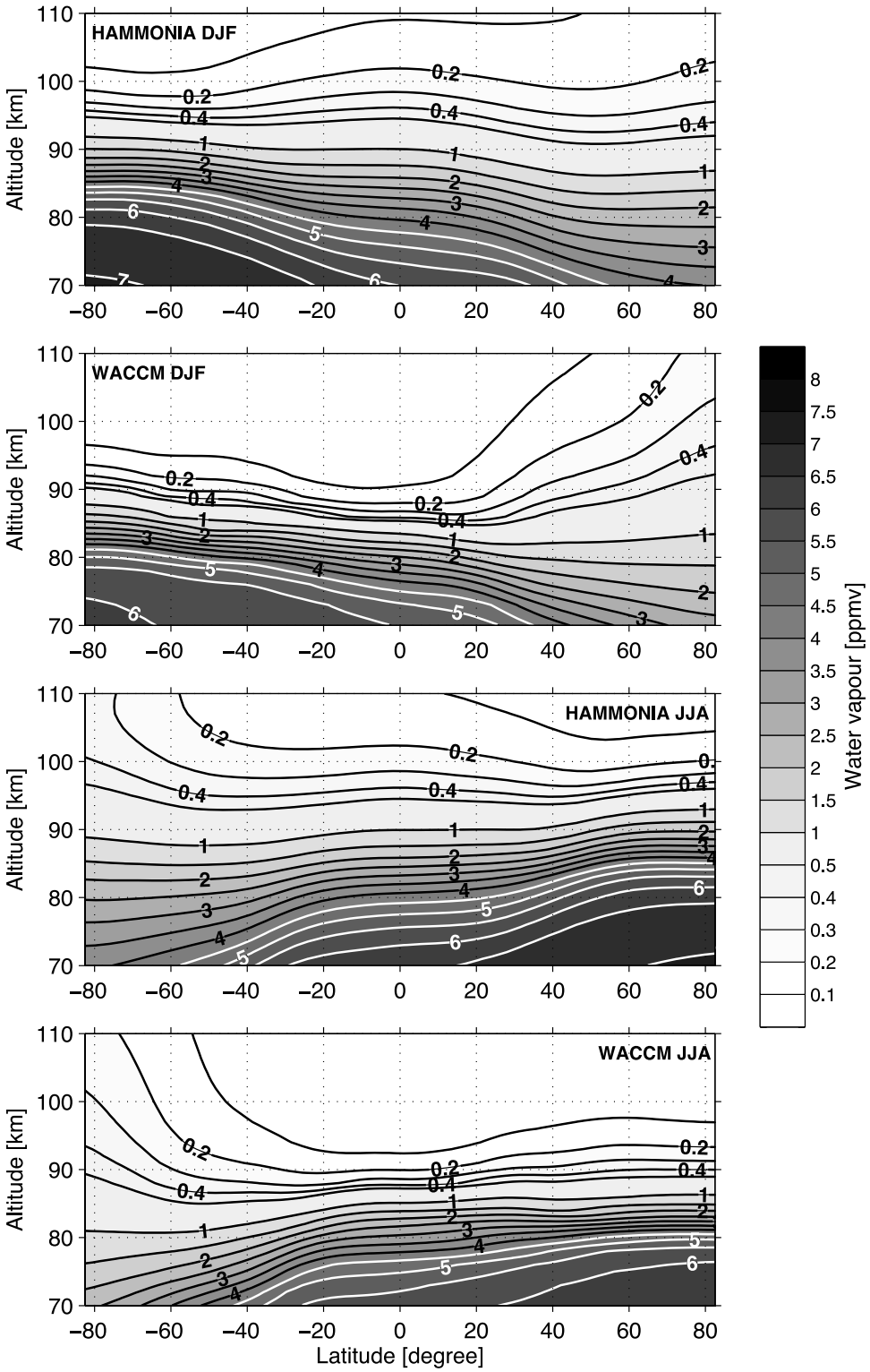

Figure 5. Like Figure 3 but here for HAMMONIA and WACCM3 results.

mesosphere and lower thermosphere. In the polar regions in both hemispheres the observations show a distinct seasonal increase of the water vapor concentration during wintertime at a given altitude above 90 km. While the Odin observations are influenced and modulated by tidal signatures owing to the local time coverage of the satellite, the model results show that this feature also appears in diurnally averaged conditions. Several contributions may give rise to this observed increase in water vapor during the winter season above 90 km.

[26] The annual distribution of mesospheric water vapor below about 90 km is essentially determined by dynamics. The gravity wave driven meridional circulation is accompanied with upwelling of moister air from below over the

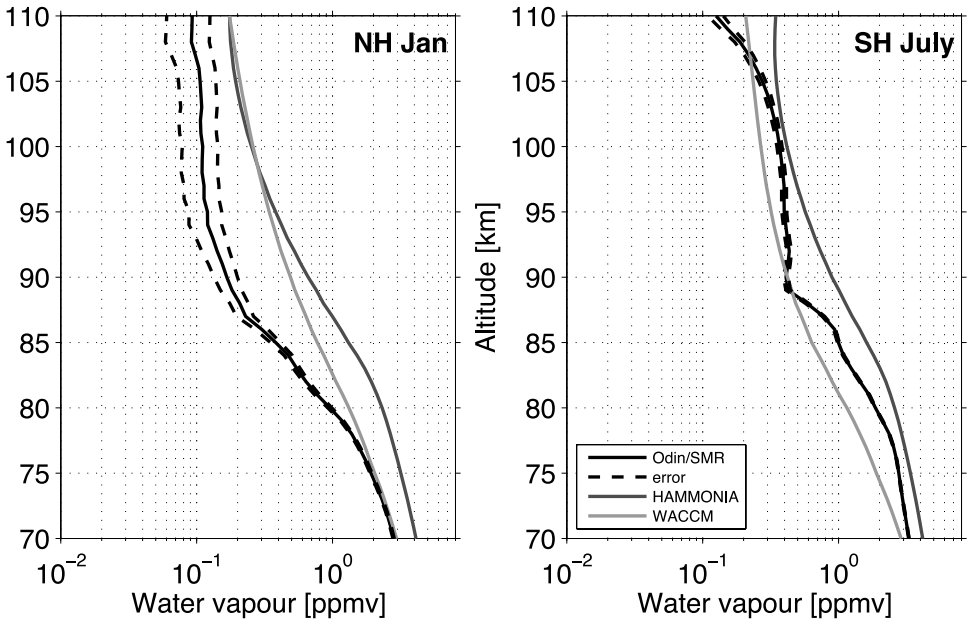

Figure 6. Comparison between Odin/SMR measurements and simulations from HAMMONIA and WACCM3. (left) Mean profiles for January in the Northern Hemisphere polar region (60° to 82.5° latitude) and (right) mean profiles for July in the polar region of the Southern Hemisphere. The dashed lines describe the statistical error range of the Odin/SMR mean profiles. Note the log scale of the water vapor concentration.

summer pole and downwelling of drier air from above over the winter pole. Hence the annual water vapor maximum can be observed during the summer season. Higher up the dynamical conditions differ from the conditions in the part of the mesosphere below. This is visible in Figure 7, which shows the annual distribution of the vertical wind in the polar region of the Northern and Southern Hemisphere, respectively, as described by HAMMONIA and WACCM3. Figure 7 shows that the vertical wind changes direction in the upper mesosphere during wintertime from downwelling inside the polar vortex to upwelling above. This is a direct result of resolved wave drag [*McLandress et al.*, 2006; *Becker*, 2008]. This change typically occurs in the altitude range between 85 km and 90 km, except in the WACCM3 results for the Northern Hemisphere where the change occurs already below 80 km. The upwelling above corresponds to an upward transport of moister air from lower altitudes, which is consistent with the observed water vapor increase during winter. The model results indicate that this upwelling starts at lower altitudes in the Northern Hemisphere as compared to its southern counterpart. In the HAMMONIA results another reversal of the vertical wind direction, from upwelling to downwelling conditions, can be observed higher up. This behavior is not captured by the WACCM3 simulations. Above the strong upwelling in the polar summer mesopause region the models exhibit downwelling conditions. The change in the vertical wind direction occurs in the altitude range between 90 km and 95 km, i.e., somewhat higher up as during wintertime. The downwelling above the summer mesopause region corresponds to a transport of drier air from above, which is also consistent with the low water vapor concentrations observed during the summer season in the lower thermosphere. We note also that the downwelling differs quite a lot in strength and appearance between the two model simulations.

[27] The relative dryness in the lowermost summertime thermosphere, i.e., in the altitude range from about 90 km up to about 95 km, might be in addition also still a consequence of the water vapor redistribution by ice particles in the summer mesopause region. Model simulations by *von Zahn and Berger* [2003] indicate a dehydration effect up to an altitude of about 94 km in the polar region. Recent measurements of the SABER (Sounding the Atmosphere using Broadband Emission Radiometry, [*Russell et al.*, 1999]) instrument aboard the TIMED (Thermosphere-Ionosphere-Mesosphere Energetics and Dynamics) satellite suggest a dehydration up to about 95 km [*Siskind et al.*, 2008]. Atomic hydrogen, inferred from those measurements, exhibits a prominent decrease in the lowermost thermosphere during summer which is most likely associated with the reduction of its chemical source water vapor caused by the redistribution process. Note that neither the HAMMONIA nor the WACCM3 simulations presented here include any representation of the ice particles and their effects on water vapor distribution in the polar summer mesopause region.

[28] In addition to the processes discussed above a certain contribution to the observations arises from the influence of the annual variation of Lyman-α flux. As described, the photodissociation of water vapor by Lyman-α radiation is the major sink for water vapor above 70 km [*Brasseur and Solomon*, 1998]. The higher the solar zenith angle the deeper Lyman-α radiation penetrates into the mesosphere and the stronger the water vapor decreases with altitude. During polar night, no direct solar Lyman-α radiation reaches the altitude range between 90 km and 110 km.

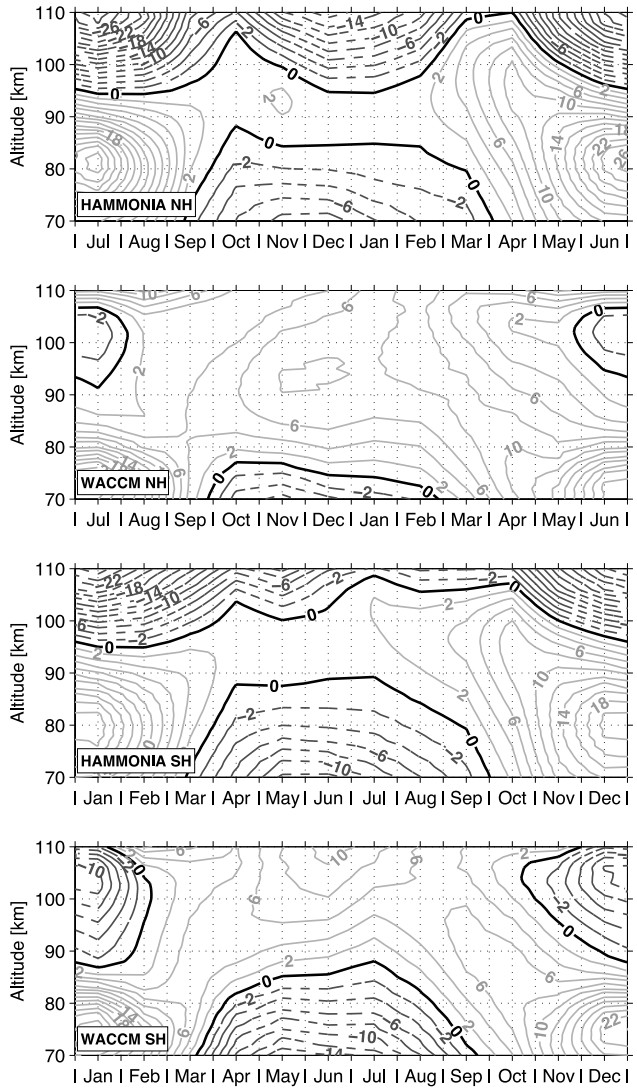

Figure 7. Annual distribution of the vertical wind in the polar area (60°–82.5° latitude) in the Northern and Southern Hemisphere from HAMMONIA and WACCM3. Positive values correspond to upwelling (light grey solid contour lines), and negative values indicate downwelling (dark grey dashed contour lines).

Instead this altitude region is illuminated only by the Lyman-α radiation resonantly scattered by hydrogen atoms (Lyman-α geocorona). This Lyman-α geocorona flux is almost independent of the solar position and typically a factor 30 smaller than the direct solar Lyman-α flux during sunlit conditions [*Meier and Mange*, 1970, 1973]. This smaller Lyman-α flux as observed during the wintertime leads to a reduced photodissociation of water vapor and thus to a slower decrease of water vapor with altitude as compared to summertime, corresponding to higher water vapor concentrations during winter. The lifetime of water vapor with respect to photodissociation by Lyman-α in the altitude range between 90 km and 110 km will increase from a few days during polar summer conditions to several tens of days during polar night. The strong increase in the water vapor lifetime occurs around a solar zenith angle of 90 degrees. The observations and model simulations exhibit the water vapor increase even before polar night conditions prevail, which implies that a reduced Lyman-α flux will not be a basic condition for the observation of the water vapor increase. However, the prolonged water vapor lifetime during polar night conditions helps to make the seasonal increase of water in the upper mesosphere and lower thermosphere during winter more clearly visible.

[29] The dynamical conditions in the upper mesosphere and lower thermosphere described above can explain the location of the annual water vapor maximum in winter. In the altitude range between 90 km and 100 km the Odin/SMR observations and also the HAMMONIA simulations show a clear semiannual circulation with maxima in the winter- and summertime and minima close to the equinoxes. This observation is however inconsistent with the prevailing annual cycle of the vertical wind. Despite downwelling in the lower thermosphere over the summer pole combined with dehydration effects due to ice particles one of the annual maxima in the water vapor distribution is maintained here. We suggest that this observation is most likely connected to diffusion effects outweighing the dynamical effects. One has to distinguish between two types of diffusion, i.e., eddy (turbulent) diffusion due to breaking gravity waves and molecular diffusion. Both play a role for the water vapor distribution in the altitude range between 90 km and 110 km. Molecular diffusion becomes increasingly important above the turbopause, typically located at about 100 km, while eddy diffusion is important below this altitude. The strength of the eddy diffusion has a semiannual variation, with maxima at the solstices and minima at the equinoxes. A strong (rapid) eddy diffusion will cause higher water vapor concentrations compared to a weak (slow) eddy diffusion at a given altitude in an altitude region where water vapor decreases with altitude. This connection between eddy diffusion and the annual cycle of water vapor has often been discussed [e.g., *Garcia and Solomon*, 1985; *Bevilacqua et al.*, 1990; *Smith and Brasseur*, 1991; *Nedoluha et al.*, 1996] and we suggest that this causes the semiannual variation observed in the water vapor distribution in the altitude range between 90 km and 100 km. Molecular diffusion on the other hand will cause a gravitational separation of the atmospheric composition above the turbopause. This separation tends to move water vapor upward in the lower thermosphere since water vapor is still light compared to the mean air molecule mass at these altitudes. This might even sustain the seasonal water vapor increase during winter at lower thermospheric altitudes, where the HAMMONIA simulations indicate downwelling conditions.

[30] The discussion above shows that dynamics and diffusion are both essential components to explain the water vapor distribution in the altitude range between 90 km and 110 km. Still the relative importance between dynamics and diffusion processes needs to be investigated more in detail.

[31] Distinct interhemispheric differences in the wintertime water vapor distribution are visible in the Odin/SMR observations at upper mesospheric and lower thermospheric altitudes. The observed seasonal water vapor increase the winter season at altitudes above 90 km is much more pronounced in the Southern Hemisphere. In this hemisphere, higher concentrations can be observed and the increase is visible over a larger latitude range. Part of the

interhemispheric differences we observe will be due to tidal modulations, since the Odin measurements cover different local times in both hemispheres. The model results, which describe diurnally averaged conditions, exhibit interhemispheric differences as well. As in the Odin/SMR observations the seasonal increase of the water vapor concentration in wintertime is much more pronounced in the Southern Hemisphere in the HAMMONIA simulations. The WACCM3 results exhibit also higher peak water vapor concentrations above 95 km during wintertime in the Southern Hemisphere, but the interhemispheric differences are evidently smaller as in the Odin and HAMMONIA results. Both interhemispheric differences in the dynamical conditions as well as in diffusion can be responsible for the interhemispheric differences observable in the polar upper mesosphere and lower thermosphere water vapor distribution during the winter season. With regard to dynamics this assumption might imply on one hand a stronger upwelling in the Southern Hemisphere polar region as compared to its northern counterpart. On the other hand also an upwelling starting at lower altitudes, resulting in an upward transport of higher water vapor concentrations, might be an explanation. These assumptions are only to a small fraction supported by the model simulations, they actually indicate much more the opposite. The upwelling in the winter season starts at lower altitudes in the Northern Hemisphere. In the altitude range between 90 km and 100 km the WACCM3 results exhibit a stronger upwelling again in the Northern Hemisphere, the upwelling is rather similar in both hemispheres in the HAMMONIA simulations. Only above 100 km the dynamical conditions would be consistent with the observed interhemispheric differences in water vapor during the winter season. The WACCM3 simulations exhibit on one hand a stronger upwelling in the Southern Hemisphere as compared to its northern equivalent in this altitude region. The HAMMONIA results on the other hand show here a weaker downwelling in the Southern Hemisphere than in the Northern Hemisphere. Both scenarios correspond to higher water vapor concentrations in the Southern Hemisphere than in the Northern Hemisphere above 100 km in wintertime. This discussion of the dynamical interhemispheric differences would suggest that the interhemispheric differences observed in the wintertime water vapor distribution in the upper mesosphere and lower thermosphere are dominated by differences in the diffusion between the two hemispheres. This implies a more rapid diffusion in the Southern Hemisphere as compared to the Northern Hemisphere. Nevertheless, it is obvious that the anticipated interhemispheric differences need a more thorough study.

[32] A rather small fraction of the interhemispheric differences in the wintertime water vapor distribution may also be explained by differences in the Lyman-α geocorona due the fact that the Sun is closer to the Earth in January than in July. This should lead to a higher Lyman-α geocorona flux during the Northern Hemisphere winter than in the Southern Hemisphere winter in the upper mesosphere and lower thermosphere, corresponding to more water vapor destruction in the Northern Hemisphere. Note that the Lyman-α geocorona flux however is not implemented in the model simulations, emphasizing once more that the interhemispheric differences in the Lyman-α geocorona flux are only of minor importance.

[33] Finally we want to note that the Odin/SMR water vapor measurements always exhibit lower concentrations as the HAMMONIA simulation in the upper mesosphere and lower thermosphere region. This also the case when comparing the measurements to the WACCM3 results in the polar area of the Northern Hemisphere in January. At the uppermost altitude addressed here, i.e., 110 km, the model results show a factor of 2–3 higher water vapor concentrations as the Odin/SMR measurements. This could be a hint of the same dry bias in the Odin/SMR water vapor data as observed in the comparison with ACE/FTS measurements below 90 km. Since the solar cycle maximum is not covered by the implemented satellite data here there is a likelihood that the Odin/SMR results should exhibit somewhat higher water vapor concentrations as the model results, which represent solar cycle average conditions (see section 4). Taking this aspect into account will increase the anticipated dry bias of the Odin/SMR measurements further. Moreover we have not accounted for any tidal effects in this comparison; however, the tidal effects are expected to be small [e.g., *Hagan et al.*, 1999] and should not change the comparison results too much. Nonetheless, it is clear that the differences between the measurements and model simulations cannot be explained by possible systematic errors of the Odin/SMR results alone, which were estimated to be on the order of 10% to 20%. On the other hand also the HAMMONIA and WACCM3 simulations exhibit obvious differences among each other. For example the increase in water vapor in the upper mesosphere and lower thermosphere is visible over a longer period of time in the WACCM3 simulations. In July in the polar area of the Southern Hemisphere the HAMMONIA simulations show water vapor concentrations typically twice as high the one from WACCM3. A similar situation is visible outside the polar winter region above 90 km. Differences between the two model can also be found in the annual distribution of the vertical wind in the polar region.

[34] **Acknowledgments.** Odin is a Swedish-led satellite project funded jointly by the Swedish National Space Board (SNSB), the Canadian Space Agency (CSA), the National Technology Agency of Finland (Tekes), and the Centre National d'Etudes Spatiales (CNES) in France. The Swedish Space Corporation has been the industrial prime constructor. Since April 2007, Odin is a third-party mission of the European Space Agency (ESA). The main author is supported by grants from SNSB. We wish to acknowledge Nicolas Lautié for his early contributions on the implementation of the 557-GHz band retrieval algorithms. The WACCM model has been developed at the National Center for Atmospheric Research (NCAR) in Boulder (Colorado), USA. The National Center for Atmospheric Research is sponsored by the National Science Foundation. We also would like to acknowledge Jonas Hedin for the Lyman-α geocorona data set and Farah Khosrawi for her comments on an early version of this manuscript.

References

Arnold, F., and D. Krankowsky (1977), Water vapour concentrations at the mesopause, *Nature*, *268*, 218–219.

Becker, E. (2008), Sensitivity of the upper mesosphere to the Lorenz energy cycle of the troposphere, *J. Atmos. Sci.*, *66*(3), 647–666, doi:10.1175/2008JAS2735.1.

Bernath, P. F., et al. (2005), Atmospheric Chemistry Experiment (ACE): Mission overview, *Geophys. Res. Lett.*, *32*, L15S01, doi:10.1029/2005GL022386.

Bevilacqua, R. M., M. E. Summers, D. F. Strobel, J. J. Olivero, and M. Allen (1990), The seasonal variation of water vapor and ozone in the upper

mesosphere: Implications for vertical transport and ozone photochemistry, *J. Geophys. Res.*, *95*, 883–893.

Boone, C. D., R. Nassar, K. A. Walker, Y. Rochon, S. D. McLeod, C. P. Rinsland, and P. F. Bernath (2005), Retrievals for the Atmospheric Chemistry Experiment Fourier-Transform Spectrometer, *Appl. Opt.*, *44*, 7218–7231.

Brasseur, G., and S. Solomon (1998), *Aeronomy of the Middle atmosphere*, D. Reidel, Dordrecht, Netherlands.

Carleer, M. R., et al. (2008), Validation of water vapour profiles from the Atmospheric Chemistry Experiment (ACE), *Atmos. Chem. Phys. Discuss.*, *8*, 4499–4559.

Chandra, S., C. H. Jackman, E. L. Fleming, and J. M. Russell III (1997), The seasonal and long term changes in mesospheric water vapor, *Geophys. Res. Lett.*, *24*, 639–642, doi:10.1029/97GL00546.

Chapman, S., and R. S. Lindzen (1970), *Atmospheric Tides*, D. Reidel, Norwell, Mass.

Ekström, M., P. Eriksson, B. Rydberg, and D. P. Murtagh (2007), First Odin sub-mm retrievals in the tropical upper troposphere: Humidity and cloud ice signals, *Atmos. Chem. Phys.*, *7*(2), 459–469.

Fischer, H., J. Gille, and J. M. Russell III (1981), Water vapor in the stratosphere—Preliminary results of the LIMS experiment aboard Nimbus 7, *Adv. Space Res.*, *1*, 279–281, doi:10.1016/0273-1177(81)90404-X.

Fleming, E., S. Chandra, J. Barnett, and M. Corney (1990), Zonal mean temperature, pressure, zonal wind, and geopotential height as functions of latitude, COSPAR International reference atmosphere: 1986, Part II: Middle atmosphere models, *Adv. Space Res.*, *10*, 11–59.

Frisk, U., et al. (2003), The Odin satellite. I. Radiometer design and test, *Astron. Astrophys.*, *402*, L27–L34, doi:10.1051/0004-6361:20030335.

Fueglistaler, S., A. E. Dessler, T. J. Dunkerton, I. Folkins, Q. Fu, and P. W. Mote (2009), Tropical tropopause layer, *Rev. Geophys.*, *47*, RG1004, doi:10.1029/2008RG000267.

Garcia, R. R., and S. Solomon (1985), The effect of breaking gravity waves on the dynamics and chemical composition of the mesosphere and lower thermosphere, *J. Geophys. Res.*, *90*, 3850–3868, doi:10.1029/JD090iD02p03850.

Garcia, R. R., D. R. Marsh, D. E. Kinnison, B. A. Boville, and F. Sassi (2007), Simulation of secular trends in the middle atmosphere, 1950–2003, *J. Geophys. Res.*, *112*, D09301, doi:10.1029/2006JD007485.

Grossmann, K. U., W. G. Frings, D. Offermann, L. André, E. Kopp, and D. Krankowsky (1985), Concentrations of H_2O and NO in the mesosphere and the lower thermosphere at high latitudes, *J. Atmos. Terr. Phys.*, *47*, 291–300.

Hagan, M. E., and J. M. Forbes (2002), Migrating and nonmigrating diurnal tides in the middle and upper atmosphere excited by tropospheric latent heat release, *J. Geophys. Res.*, *107*(D24), 4754, doi:10.1029/2001JD001236.

Hagan, M. E., and J. M. Forbes (2003), Migrating and nonmigrating semidiurnal tides in the upper atmosphere excited by tropospheric latent heat release, *J. Geophys. Res.*, *108*(A2), 1062, doi:10.1029/2002JA009466.

Hagan, M. E., M. D. Burrage, J. M. Forbes, J. Hackney, W. J. Randel, and X. Zhang (1999), GSWM-98: Results for migrating solar tides, *J. Geophys. Res.*, *104*, 6813–6828, doi:10.1029/1998JA900125.

Hervig, M., M. McHugh, and M. E. Summers (2003), Water vapor enhancement in the polar summer mesosphere and its relationship to polar mesospheric clouds, *Geophys. Res. Lett.*, *30*(20), 2041, doi:10.1029/2003GL018089.

Holton, J. R., P. H. Haynes, M. E. McIntyre, A. R. Douglass, R. B. Rood, and L. Pfister (1995), Stratosphere-troposphere exchange, *Rev. Geophys.*, *33*, 403–439.

Killeen, T. L., Q. Wu, S. C. Solomon, D. A. Ortland, W. R. Skinner, R. J. Niciejewski, and D. A. Gell (2006), TIMED Doppler Interferometer: Overview and recent results, *J. Geophys. Res.*, *111*, A10S01, doi:10.1029/2005JA011484.

Kopp, E. (1990), Hydrogen constituents of the mesosphere inferred from positive ions: H_2O, CH_4, H_2CO, H_2O_2, and HCN, *J. Geophys. Res.*, *95*, 5613–5630, doi:10.1029/JD095iD05p05613.

Lossow, S., J. Urban, P. Eriksson, D. Murtagh, and J. Gumbel (2007), Critical parameters for the retrieval of mesospheric water vapour and temperature from Odin/SMR limb measurements at 557 GHz, *Adv. Space Res.*, *40*, 835–845.

McLandress, C., W. E. Ward, V. I. Fomichev, K. Semeniuk, S. R. Beagley, N. A. McFarlane, and T. G. Shepherd (2006), Large-scale dynamics of the mesosphere and lower thermosphere: An analysis using the extended Canadian Middle Atmosphere Model, *J. Geophys. Res.*, *111*, D17111, doi:10.1029/2005JD006776.

Meier, R. R., and P. Mange (1970), Geocoronal hydrogen: An analysis of the Lyman-alpha airglow observed from OGO-4, *Planet. Space Sci.*, *18*, 803–821.

Meier, R. R., and P. Mange (1973), Spatial and temporal variations of the Lyman-alpha airglow and related atomic hydrogen distributions, *Planet. Space Sci.*, *21*, 309–327, doi:10.1016/0032-0633(73)90030-5.

Mote, P. W., K. H. Rosenlof, M. E. McIntyre, E. S. Carr, J. C. Gille, J. R. Holton, J. S. Kinnersley, H. C. Pumphrey, J. M. Russell III, and J. W. Waters (1996), An atmospheric tape recorder: The imprint of tropical tropopause temperatures on stratospheric water vapor, *J. Geophys. Res.*, *101*, 3989–4006, doi:10.1029/95JD03422.

Nassar, R., P. F. Bernath, C. D. Boone, G. L. Manney, S. D. McLeod, C. P. Rinsland, R. Skelton, and K. A. Walker (2005), ACE-FTS measurements across the edge of the winter 2004 Arctic vortex, *Geophys. Res. Lett.*, *32*, L15S05, doi:10.1029/2005GL022671.

Nedoluha, G. E., R. M. Bevilacqua, R. Michael Gomez, W. B. Waltman, B. C. Hicks, D. L. Thacker, and W. Andrew Matthews (1996), Measurements of water vapor in the middle atmosphere and implications for mesospheric transport, *J. Geophys. Res.*, *101*, 21,183–21,194, doi:10.1029/96JD01741.

Randel, W. J., F. Wu, J. M. Russell III, A. Roche, and J. W. Waters (1998), Seasonal cycles and QBO variations in stratospheric CH_4 and H_2O observed in UARS HALOE data, *J. Atmos. Sci.*, *55*, 163–185.

Reber, C. A., C. E. Trevathan, R. J. McNeal, and M. R. Luther (1993), The Upper Atmosphere Research Satellite (UARS) mission, *J. Geophys. Res.*, *98*, 10,643–10,648.

Remsberg, E., J. M. Russell III, L. L. Gordley, J. C. Gille, and P. L. Bailey (1984), Implications of the stratospheric water vapor distribution as determined from the Nimbus 7 LIMS experiment, *J. Atmos. Sci.*, *41*, 2934–2948.

Rodgers, C. D. (2000), *Inverse Methods for Atmospheric Soundings: Theory and Practice*, World Sci., Hackensack, N. J.

Russell, J. M., III, M. G. Mlynczak, L. L. Gordley, J. J. Tansock, and R. W. Esplin (1999), Overview of the SABER experiment and preliminary calibration results, *Proc. SPIE Int. Soc. Opt. Eng.*, *3756*, 277–288.

Schmidt, H., G. P. Brasseur, M. Charron, E. Manzini, M. A. Giorgetta, T. Diehl, V. I. Fomichev, D. Kinnison, D. Marsh, and S. Walters (2006), The HAMMONIA chemistry climate model: Sensitivity of the mesopause region to the 11-year solar cycle and CO_2 doubling, *J. Clim.*, *19*, 3903–3931, doi:10.1175/JCLI3829.1.

Seele, C., and P. Hartogh (1999), Water vapor of the polar middle atmosphere: Annual variation and summer mesosphere conditions as observed by ground-based microwave spectroscopy, *Geophys. Res. Lett.*, *26*, 1517–1520, doi:10.1029/1999GL900315.

Siskind, D. E., D. R. Marsh, M. G. Mlynczak, F. J. Martin-Torres, and J. M. Russell III (2008), Decreases in atomic hydrogen over the summer pole: Evidence for dehydration from polar mesospheric clouds?, *Geophys. Res. Lett.*, *35*, L13809, doi:10.1029/2008GL033742.

Smith, A. K., and G. P. Brasseur (1991), Numerical simulation of the seasonal variation of mesospheric water vapor, *J. Geophys. Res.*, *96*, 7553–7563, doi:10.1029/91JD00226.

Sonnemann, G. R., and M. Grygalashvyly (2005), Solar influence on mesospheric water vapor with impact on NLCs, *J. Atmos. Solar Terr. Phys.*, *67*, 177–190, doi:10.1016/j.jastp.2004.07.026.

Sonnemann, G. R., M. Grygalashvyly, and U. Berger (2005), Autocatalytic water vapor production as a source of large mixing ratios within the middle to upper mesosphere, *J. Geophys. Res.*, *110*, D15303, doi:10.1029/2004JD005593.

Summers, M. E., R. R. Conway, D. E. Siskind, M. H. Stevens, D. Offermann, M. Riese, P. Preusse, D. F. Strobel, and J. M. Russell III (1997), Implications of satellite OH observations for middle atmospheric H_2O and ozone, *Science*, *277*, 1967–1970.

Summers, M. E., L. L. Gordley, and M. J. McHugh (2001), Discovery of a water vapor layer in the Arctic summer mesosphere: Implications for polar mesospheric clouds, *Geophys. Res. Lett.*, *28*, 3601–3604, doi:10.1029/2001GL013217.

Taylor, F. W., J. J. Barnett, I. Colbeck, R. L. Jones, C. D. Rodgers, M. J. Wale, and E. J. Williamson (1981), Performance and early results from the Stratospheric and Mesospheric Sounder (SAMS) on Nimbus 7, *Adv. Space Res.*, *1*, 261–265, doi:10.1016/0273-1177(81)90068-5.

Thomason, L. W., S. P. Burton, N. Iyer, J. M. Zawodny, and J. Anderson (2004), A revised water vapor product for the Stratospheric Aerosol and Gas Experiment (SAGE) II version 6.2 data set, *J. Geophys. Res.*, *109*, D06312, doi:10.1029/2003JD004465.

Urban, J., et al. (2005), Odin/SMR limb observations of stratospheric trace gases: Level 2 processing of ClO, N_2O, HNO_3, and O_3, *J. Geophys. Res.*, *110*, D14307, doi:10.1029/2004JD005741.

Urban, J., et al. (2007), Global observations of middle atmospheric water vapour by the Odin satellite: An overview, *Planet. Space Sci.*, *55*, 1093–1102, doi:10.1016/j.pss.2006.11.021.

von Zahn, U., and U. Berger (2003), Persistent ice cloud in the midsummer upper mesosphere at high latitudes: Three-dimensional modeling and

cloud interactions with ambient water vapor, *J. Geophys. Res.*, *108*(D8), 8451, doi:10.1029/2002JD002409.

Wu, Q., T. L. Killeen, D. A. Ortland, S. C. Solomon, R. D. Gablehouse, R. M. Johnson, W. R. Skinner, R. J. Niciejewski, and S. J. Franke (2006), TIMED Doppler Interferometer (TIDI) observations of migrating diurnal and semi-diurnal tides, *J. Atmos. Solar Terr. Phys.*, *68*, 408–417, doi:10.1016/j.jastp.2005.02.031.

P. Eriksson, S. Lossow, D. Murtagh, and J. Urban, Department of Radio and Space Science, Chalmers University of Technology, Hörsalsvägen 11, SE-41296 Göteborg, Sweden. (patrick.eriksson@chalmers.se; stefan.lossow@misu.su.se; donal.murtagh@chalmers.se; joaurb@chalmers.se)

J. Gumbel, Department of Meteorology, Stockholm University, Svante-Arrhenius-väg 12, SE-10691 Stockholm, Sweden. (gumbel@misu.su.se)

D. R. Marsh, Atmospheric Chemistry Division, National Center for Atmospheric Research, 3450 Mitchell Lane, Boulder, CO 80301, USA. (marsh@ucar.edu)

H. Schmidt, Atmosphere in the Earth System, Max Planck Institute for Meteorology, Bundesstraße 53, D-20146 Hamburg, Germany. (hauke.schmidt@zmaw.de)